

Noisy Neighbor Influence in the Data Plane of Beyond 5G Networks

Rodrigo Moreira¹, Larissa Ferreira Rodrigues Moreira¹, Tereza C. Carvalho², Flávio de Oliveira Silva³

¹Federal University of Viçosa (UFV), Minas Gerais, Brazil

²University of São Paulo (USP), São Paulo, Brazil

³University of Minho (UMinho), Braga, Portugal

Emails: rodrigo@ufv.br, larissa.f.rodrigues@ufv.br, terezacarvalho@usp.br, flavio@di.uminho.pt

Abstract—Virtualization and containerization enhance the modularity and scalability of mobile network architectures, facilitating customized user services and improving management and orchestration across the network. In the context of the 5th Generation Mobile Network (5G), these advancements contribute to reduced Operational Expenditures (OPEX) and enable sliced-based networking for novel applications and services. However, as beyond fifth-generation (B5G) networks aim to address the remaining challenges regarding network slice isolation, the shared underlying hardware can lead to data plane contention among slices, resulting in the Noisy Neighbor (NN) effect, which may compromise network slicing and Service-Level Agreements (SLAs). We propose a kernel-level instrumentation of the User Plane Function (UPF) to assess the impact of noisy slices on data plane processing. Our findings reveal that even prioritized slices are susceptible to degradation induced by NN, with observable effects on latency metrics pertinent to user experience.

Index Terms—B5G, Noisy Neighbor, UPF Instrumentation, Slice Isolation, Data-Plane Latency.

I. INTRODUCTION

Cloud computing employs virtualization and containerization to deliver multi-tenant isolation and efficient resource use; the rise of microservices and serverless computing further increases consolidation density, operational agility, and the pace of cloud-native innovation [1]–[5]. This paradigm has reshaped mobile network architectures, such as those of 5th Generation Mobile Network (5G) and emerging Beyond Fifth Generation (B5G), enabling them to adopt cloud-native designs from the core to the access point and decompose network functions into modular microservices [6]. The result is fine-grained scaling and lower Operating Expenditures (OPEX), but also greater susceptibility to cross-tenant performance interference or noise effects [7], [8]. Even slices engineered with Service-Level Agreement (SLA) guarantees can face resource contention that weakens isolation in practice [5], [7], [9].

The Noisy Neighbor (NN) effect occurs when aggressive co-tenants exhaust shared resources and remains a major source of cross-tenant interference in virtualized environments [8], from 5G core microservices to virtualized baseband, despite Central Processing Unit (CPU) pinning, cgroup limits, and cache partitioning. Its impact manifests most intensely in the user plane, where latency spikes and heavy tails erode slice-based differentiation [10], [11]. Despite prior work on detection and mitigation in cloud and telecom, there is little kernel-level, per-packet evidence of how NNs perturb the mobile data

plane, especially within the User Plane Function (UPF) during General Packet Radio Service Tunnelling Protocol User Plane (GTP-U) decapsulation. Methods based on aggregate throughput, queue counters, or offline profiling miss microbursts and cannot attribute latency to specific kernel stages [5], [7], [11], [12].

We propose kernel instrumentation to measure and attribute the GTP-U decapsulation overhead in a container-based UPF on Kubernetes. Using bpftrace, an Extended Berkeley Packet Filter (eBPF), the probe timestamps at the General Packet Radio Service Tunnelling Protocol (GTP) module entry and at `net_if_rx` are used to compute the per-packet decapsulation latency. It filters a target User Equipment (UE) Internet Protocol (IP) to isolate a sensor flow and tags each sample with a Tunnel Endpoint Identifier (TEID)/Quality of Service Flow Identifier (QFI) context. The result is high-resolution latency traces that reveal how competing flows and co-located workloads modulate the decapsulation cost across traffic classes and slice priorities.

Our main contributions are as follows: (i) we introduce lightweight, kernel-level per-packet instrumentation for the UPF GTP-U decapsulation that attributes data-plane latency to specific TEID/QFI flows; (ii) we provide a compact analysis framework with robust summaries and nonparametric tests to quantify the impact of the NN on median and tail latencies; (iii) we present empirical evidence that disruptive co-located workloads inflate decapsulation latency even for high-priority QFIs, revealing the limits of slice isolation; and (iv) we distill operator guidance for telemetry and orchestration (what to monitor, how to flag early degradation, and how to prioritize mitigation). Our diagnostic framework lays the foundation for runtime mitigation strategies.

The remainder of this paper is organized as follows: section II reviews interference and NN literature across cloud and mobile networks. Section III details our proposed method. Section IV presents the testbed and evaluation scenarios. Section V presents the results and discussion, and Section VI draws conclusions and outlines future work.

II. RELATED WORK

This section highlights several studies that focused on implementing and examining the impact of simultaneous applications in virtualized or containerized settings. Finally, we

TABLE I: Comparison of related work.

Approach	5GC	UPF	RAN	NN focus	Online detect.	Mitigation	eBPF	Per-packet (kernel)	K8s-based	Open-src	CP focus
Mukute et al. [13]	●	○	○	○	○	○	●	○	○	●	●
Volpert et al. [11]	○	○	○	●	●	○	●	○	○	○	○
Muro et al. [7]	●	○	○	●	○	●	○	○	○	○	●
Andrade et al. [14]	●	●	○	○	○	●	○	○	●	●	○
Adeppady et al. [15]	○	○	○	●	○	●	○	○	●	○	○
Da Silva et al. [16]	●	○	○	○	○	○	○	○	●	○	●
Lozano et al. [8]	○	○	●	●	●	●	○	○	○	○	○
Ours	●	●	○	●	○	○	●	●	●	●	○

present our findings in a comparative table that motivates our instrumentation method.

Mukute et al. [13] provide a control plane centered, feature grounded comparison of open source 5G cores by mapping network function operations to 5G procedures and combining macro benchmarking with micro benchmarking using a custom UE traffic generator and eBPF profiling. They report end to end registration times and per process system call latency and frequency with attribution, show correlation between macro and micro signals that reveals optimization points, and release practical recommendations and replication artifacts.

Volpert et al. [11] study interference that persists under CPU cgroup isolation and the limits of detectors that depend on workload profiles or offline analysis. They instrument the Linux scheduler with eBPF tracepoints and define two online, workload agnostic metrics, Average Process Scheduling Latency and Average Process Scheduler Preemptions, plus a decision matrix. Across eight contention scenarios on Kubernetes and Argo with stress-ng and nsjail, the metrics track resource isolation and application quality of service, detect noisy neighbors online without per workload models, and separate them from self disruption.

Muro et al. [7] build a core focused testbed to quantify noisy neighbor effects in virtualized 5G cores, emulating a full core and creating a cpulimit based simulator that throttles the LoadCore agent. A factorial campaign with and without a noisy neighbor varies packet rate, packet size, and number of UE; they collect throughput, delay, loss, and core CPU, train cross validated classifiers, identify packet rate as the dominant driver of core CPU demand, and observe throughput reduction with higher delay and loss under noise.

Andrade et al. [14] evaluate slice isolation controls for private 5G cores on cloud and edge platforms, testing Kubernetes and Linux mechanisms at the UPF: CPU requests and limits with cgroups, Cilium earliest departure time bandwidth control, and process priority via nice, alone and in combination. In a hospital video conferencing scenario with a prioritized slice under growing background load, 26 experiments with 10 runs and Prometheus telemetry show that CPU caps on non priority slices consistently improve the prioritized slice, while bandwidth caps are powerful but can starve others if set too strictly.

Adeppady et al. [15] design iPlace, a Kubernetes placement heuristic that clusters microservices by contention dissimilarity

and enables batch deployment. Using testbed pairwise interference measurements and simulations against several baselines, iPlace approaches optimal solutions, uses between 21 percent and 92 percent fewer servers, and reduces deployment time by 69 percent.

Da Silva et al. [16] pursue low overhead, real time estimation of user experience in container based 5G cores. Deploying free5GC on Kubernetes and applying stochastic CPU, memory, and network stress with Chaos Mesh while issuing continuous registrations, they learn regressors from generic infrastructure metrics to registration latency on a FABRIC testbed with a 24 hour cyclic pattern. Random Forest (RF) achieves approximately 10.5 percent Mean Absolute Percentage Error (MAPE) with a top ten feature subset, which also reduces runtime, outperforming K-Nearest Neighbors (KNN), Decision Tree (DT), Support Vector Machine (SVM), and Long Short-Term Memory (LSTM) in this setting.

Lozano et al. [8] examine noisy neighbor effects in shared virtual Radio Access Network (RAN). On a Dockerized srsRAN testbed they quantify overhead sources including hyper threading, namespaces, seccomp, context switches, and cache contention, then propose an Open Radio Access Network (O-RAN) compliant non real time RAN Intelligent Controller (RIC) policy that uses a Relation Network encoder with a Deep Q-Network (DQN) to select the number of active cores. With two to five virtual base stations under maximum load and five-day traces, they measure throughput, CPU assignment, power, instructions per cycle, cache misses, and inference time, identify cache contention as the dominant bottleneck, and show that the policy reaches near oracle performance with up to 30 percent resource savings and about 99.9 percent availability.

Table I contrasts prior work and ours using binary features, where a filled circle (●) denotes “Yes” and a hollow circle (○) denotes “No”. The second column (5GC) indicates work targeting the 5G Core; UPF flags user plane processing; RAN marks radio-access analysis; NN focus denotes explicit treatment of noisy-neighbor interference; Online detect. indicates run-time detection; Mitigation means the work proposes or evaluates countermeasures; eBPF captures the use of kernel observability via eBPF/Berkeley Packet Filter (BPF) toolchains; Per-packet (kernel) means kernel-space, per-packet telemetry/instrumentation; K8s-based signals

experimentation/deployment on Kubernetes; Open-src denotes released artifacts enabling reproduction; and Control Plane (CP) highlights a predominant control-plane orientation (as opposed to data-plane).

Positioning. Prior work spans control plane comparisons, scheduler detectors, slice controls, placement, and user experience prediction at aggregate timescales; we provide kernel level, per packet attribution of UPF GTP-U decapsulation latency under coexisting TEID and QFI flows, revealing microbursts and limits of slice isolation that aggregate counters cannot see.

III. PROPOSED METHOD

Quantifying the mutual effects of 5G slices on the data plane is challenging, especially in terms of processing cost and traffic isolation between network slices. We propose a kernel-level bpftrace instrumentation to measure the per-packet overhead of GTP-U decapsulation in the UPF. As in Fig. 1, we timestamp packets at the entry of `gtp5g_handle_skb_ipv4` (decapsulation) and again at `netif_rx`; their difference is the decapsulation latency. As depicted in Fig. 1, within the UPF, the N3 interface serves as the entry point for marking in-kernel packets. Internally, we measured various function callbacks to determine the time elapsed between GTP processing and `netif_rx` towards N6. The N2 and N4 interfaces constitute the control plane interfaces of the 5G core, whereas N3 functions as the ingress user data interface.

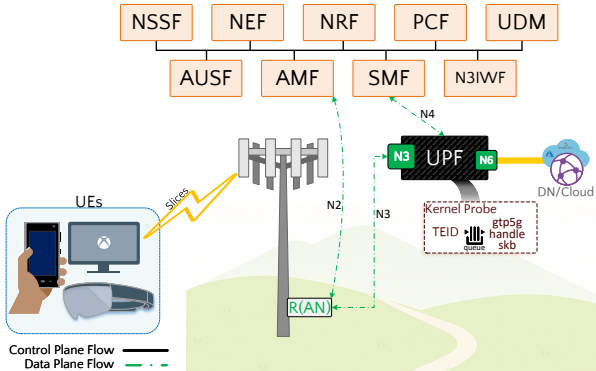


Fig. 1: Proposed Instrumentation Method.

Our proposed probe¹ filters only packets whose inner UE IP matches a configured sensor UE set by the experimenter. On match, it stores `nsecs` and the IP in BPF maps keyed by the `sk_buff` pointer; when the same `skb` reaches `netif_rx`, it computes Δt and emits “UE IP: IP_{ue} — Decapsulation Overhead: Δt ns,” then clears the entries. This lightweight design yields high resolution latency for each TEID flow and enables a precise evaluation of the NN interference in multi-TEID environments. The procedure is summarized in Algorithm 1.

¹The source code for our proposed approach is accessible at https://github.com/romoreira/5GNF_NoisyNeighbor.

Algorithm 1: Per packet GTP-U decapsulation overhead via `bpftrace`

Input: Target UE IP IP_{target}

Output: Overhead (ns) for matching packets

```

1 kprobe gtp5g_handle_skb_ipv4: parse inner
  UE IP at skb->data+8 as  $IP_{ue}$ ; if  $IP_{ue} = IP_{target}$ 
  then set @start[skb]=nsecs, @ip[skb]=IP_{ue}.
2 kprobe netif_rx: if @start[skb] exists then let
   $t = @start[skb]$ ,  $IP_{ue} = @ip[skb]$ , and
   $\Delta t = nsecs - t$ ; print  $(IP_{ue}, \Delta t)$ ; delete
  @start[skb], @ip[skb].

```

A. Influence of Noisy Neighbors on Slice Isolation

In 5G, each UE data session forms a Packet Data Unit (PDU) session with a tunnel identified by a unique TEID, allowing the UPF to map user traffic to the correct GTP-U tunnel. Within a PDU session, the QFI labels the Quality of Service (QoS) flow and is bound to the TEID and UE, so each stream receives its intended treatment. In practice, however, our method enables assessment of whether high QFI reservations and isolation are guaranteed.

Therefore, we varied the traffic classes and flow characteristics to induce “noisy neighbors” competing slices that create substantial loads or unpredictable bursts, and measured per-packet decapsulation latency across multiple TEID flows. This helps us see how well we can keep these flows separate and check if flows with strict QoS settings are protected from these noisy neighbors.

B. Statistical Analysis

To measure the influence inter 5G slices on container-based environments, we use statistical techniques as follows. For each UE traffic pattern and QFI, we summarize per-packet decapsulation latency with the median, p90, p95, p99, Interquartile Range (IQR), and Median Absolute Deviation (MAD). Pairwise comparisons against *Baseline* use two-sided Mann-Whitney U tests for median differences. In addition, permutation tests with 10^4 resamples assess Δ median and Δ p95, and bias-corrected and accelerated (BCa) bootstrap 95% confidence intervals are reported for both.

Effect sizes are given by Cliff’s δ ,

$$\delta = \frac{\#(x > y) - \#(x < y)}{n_x n_y},$$

where x and y are latency samples from the two groups (Baseline as reference vs. each alternative pattern: *Anomaly*, *Constant-Rate*, *Multimedia*).

To model distributional effects, we fit quantile regressions at $\tau \in \{0.50, 0.95, 0.99\}$ (median, high tail, extreme tail):

$$Q_\tau(\Delta t | \mathbf{x}) = \beta_0 + \beta_1 \text{CPU} + \beta_2 \text{Packets}$$

$$+ \sum_{q \in Q} \beta_{3,q} \mathbb{I}[\text{QFI} = q] + \sum_{c \in \mathcal{C}} \gamma_c \mathbb{I}[\text{Traffic} = c] \quad (1)$$

where Δt is GTP-U decapsulation latency in ns, CPU is the instantaneous UPF CPU utilization (%), and Packets is the instantaneous packet rate (pps). Q is the set of observed QFIs; $\mathcal{C} = \{\text{Baseline}, \text{Anomaly}, \text{Constant-Rate}, \text{Multimedia}\}$. The coefficients are estimated separately for each τ . Quantile regression is preferred to mean-based models because data-plane latencies are skewed and heavy-tailed; upper quantiles (p95, p99) better capture QoS behavior.

IV. EVALUATION SETUP

We ran experiments on the FABRIC testbed [17] using a virtual machine with 32vCPUs and 32GB RAM. The stack was Ubuntu + Kubernetes v1.28.15, with Free5GC emulating the 5G core. We monitored system resources with Netdata (network/Input/Output (I/O)) and pidstat for per-process CPU. To avoid bias, the containerized UPF was pinned to a single CPU core.

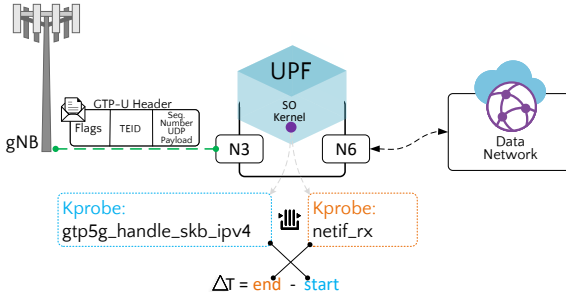


Fig. 2: Experimental setup and placement of our instrumentation within the UPF data path.

As shown in Fig. 2, the UPF was instrumented with eBPF probes to measure per-packet latency from ingress at the N3 interface to post-decapsulation delivery on eth0 (N6). Traffic was generated by a 5G traffic tool emitting GTP-U packets with valid TEIDs and QFIs across distinct patterns: Constant Bit Rate (CBR) and Packet Capture (PCAP) replays of multimedia applications (Table II). Future patterns such as Ultra-Reliable and Low Latency Communications (URLLC) and massive Internet of Things (IoT) are out of this scope. All replay traces were 100% User Datagram Protocol (UDP) with no Real-time Transport Protocol (RTP) streams detected.

TABLE II: Replayed multimedia PCAPs (Data in MiB; Avg in Mb/s).

Application	Dur (s)	Pkts (k)	Data (MiB)	Avg (Mb/s)	Pps	Mean (B)
Facebook	43.8	13.2	14.7	2.8	300.5	1171
Instagram	66.1	27.1	30.9	3.9	410.8	1193
LinkedIn	70.1	12.5	11.1	1.3	178.1	929
PS Now	59.4	17.5	15.1	2.1	294.2	906
Spotify	146.3	34.9	28.1	1.6	238.8	842
TikTok	63.9	40.7	37.8	5.0	638.0	974
Twitter	68.9	13.0	12.0	1.5	188.4	967
Wikipedia	77.4	4.8	4.1	0.4	62.3	883
YouTube	63.4	14.2	16.6	2.2	224.0	1226

We established PDU sessions in advance to ensure proper UPF processing. NN scenarios were created by co-locating

additional active PDU sessions on the same UPF to stress its CPU and I/O, while monitoring by a PDU sensor. Two scenarios were evaluated: (i) a sensor UE with a TEID mapped to a high-priority QFI while replaying diverse neighbor traffic (Table III) and (ii) the same sensor UE bound to a low-priority QFI. Each neighbor had a valid TEID and active PDU session, forcing the traversal of `gtp5g_handle_skb_ipv4`. The sensor UE sent fixed-rate Internet Control Message Protocol (ICMP) probes, and we correlated timestamped per-packet latencies with concurrent compute and network metrics to assess the impact of different neighbor priorities.

V. RESULTS AND DISCUSSION

We evaluated our method using a real 5G testbed core and instrumented the UPF with our per-packet probe from Section III. We analyzed decapsulation latency across traffic classes and QoS flows, tested differences against the *Baseline*, and modeled distributional effects with quantile regression.

A. Descriptive Analysis

Table III summarizes UPF latency by UE traffic. Baseline (ICMP) has median 16.33ns (p95 28.23ns). Anomaly is similar in center/tail but more dispersed (IQR 10.68ns vs. 4.19ns). Constant-Rate CBR is lower (median 12.75ns; p95 23.62ns), while Multimedia lies between them (median 14.88ns; p95 19.32ns). The QFI breakdown (Table IV) shows heterogeneity: QFI 9 has a slightly higher median than QFI 1 but a lower p95 value.

TABLE III: Latency summary by UE Traffic class. Values in ns.

UE Traffic	n	Median	p90	p95	p99	IQR
Anomaly	60	16.14	26.33	28.62	38.46	10.68
Baseline	60	16.33	23.33	28.23	31.35	4.19
Constant-Rate	60	12.75	17.97	23.62	27.99	4.01
Multimedia	60	14.88	18.93	19.32	22.90	4.74

The QFI-level breakdown (Table IV) reveals that QFI 9 presents a slightly higher median latency than QFI 1, but a lower p95 value, suggesting heterogeneous effects worth further modeling.

TABLE IV: Latency summary by QFI. Values in ns.

QFI	n	Median	p90	p95	p99	IQR
1	120	14.35	25.11	27.49	31.88	6.59
9	120	15.27	19.28	22.66	33.09	5.24

B. Group Comparisons

Here, we report on whether traffic patterns materially shifted user-plane latency and thus affected slice isolation, and we compared each class to the baseline. Permutation tests (10^4 resamples), Mann-Whitney U, and Cliff's δ (Table V) indicate: *Anomaly* vs. *Baseline* with no significant change. *Constant-Rate* reduces median by -3.58 ns ($p < 10^{-3}$; $\delta = -0.48$, large). *Multimedia* yields a moderate median reduction

(-1.45ns , $p \approx 0.038$) and a significant p95 decrease (-8.91ns , $p \approx 0.014$; $\delta = -0.27$, small). Detailed intervals (Table V): *Constant-Rate* $\Delta\text{median} -3.576\text{ns}$ [95% CI $-4.950, -2.299$]; *Multimedia* $\Delta\text{median} -1.452\text{ns}$ [$-2.772, -0.475$], $\Delta\text{p95} -8.907\text{ns}$ [$-11.752, -1.519$]. *Anomaly* effects are negligible.

TABLE V: Baseline vs. other traffic classes: effect sizes and statistical tests.

Comparison	ΔMedian	p_{perm}	Δp95	p_{perm}	MW p	δ	Magnitude
Anomaly	-0.19	0.91	0.39	0.87	0.688	0.043	negligible
Const.-Rate	-3.58	0.0002	-4.61	0.27	5×10^{-6}	-0.484	large
Multimedia	-1.45	0.038	-8.91	0.014	0.011	-0.269	small

C. Quantile Regression Analysis

To reveal which factors drive typical and tail latency, we model the full conditional distribution via quantile regression at $\tau \in \{0.50, 0.95, 0.99\}$ (Table VI) include UPF CPU, packet rate, QFI, and traffic class as predictors. Quantile models at $\tau \in \{0.50, 0.95, 0.99\}$ (Table VI) include UPF CPU, packet rate, QFI, and traffic dummies. CPU had a negative association with latency at p50 (-1.28ns , $p \approx 0.016$) and p95 (-4.10ns , $p \approx 0.038$), indicating better tail behavior with more CPU, whereas packets were not significant. QFI 9 is marginal at p50. *Constant-Rate* and *Multimedia* coefficients are strongly negative at p50/p95, aligning with non-parametric tests. p99 shows convergence limits (extreme-tail sparsity); increasing `max_iter` or simplifying the model mitigated this.

TABLE VI: Quantile regression coefficients (ns) and p -values for selected predictors.

Quantile	n	CPU	Packets	QFI ₉	Const.-Rate
p50	240	$\beta = -1.28$ $p = 0.016$	$\beta = 0.86$ $p = 0.361$	$\beta = 1.16$ $p = 0.066$	$\beta = -3.08$ $p < 0.001$
p95	240	$\beta = -4.10$ $p = 0.038$	$\beta = 4.69$ $p = 0.120$	$\beta = 0.56$ $p = 0.740$	$\beta = -10.31$ $p < 0.001$
p99	240	$\beta = -4.77$ $p = -$	$\beta = 2.84$ $p = -$	$\beta = -0.12$ $p = -$	$\beta = -19.02$ $p = -$

D. Visualization Analysis

Empirical Cumulative Distribution Functions (ECDFs) (Fig. 3a) show the tightest distribution for *Constant-Rate*, followed by *Multimedia*; *Anomaly* tracks *Baseline* with a slightly heavier tail, matching Table III. Violin plots (Fig. 3b) confirm the asymmetry and long upper tails, which are most visible for bursty traffic. The CPU-latency scatter with Locally Weighted Scatterplot Smoothing (LOWESS) (Fig. 3c) exhibits a downward trend and a much larger variance at low CPU, consistent with the negative CPU coefficients.

E. Discussion and Insights

The results support the hypothesis that traffic patterns significantly influence UPF processing latency, particularly in the upper quantiles.

Predictability improves latency. Constant-rate traffic not only lowers the median but also shows the largest tail latency

improvements, likely owing to its predictable nature, which enables better CPU scheduling and queue management. The Empirical Cumulative Distribution Function (ECDF) (Fig. 3a) and violin plots (Fig. 3b) further illustrates this effect, with *Constant-Rate* exhibiting a narrow, steep distribution and minimal upper-tail elongation.

Moderate traffic, moderate gains. Multimedia traffic also benefits from reduced latency, although to a lesser extent. The violin plot (Fig. 3b) reveals a moderate spread with a less pronounced tail than *Baseline*, confirming its intermediate position between highly predictable and bursty patterns. The negligible effect of *Anomaly* Traffic is consistent across the ECDF (Fig. 3a) and violin plots (Fig. 3b) visualizations, where its curve and density shape remain close to the *Baseline* but with a slightly heavier tail, suggesting that the current resource isolation and scheduling mechanisms can absorb bursty interference without major degradation in the data plane.

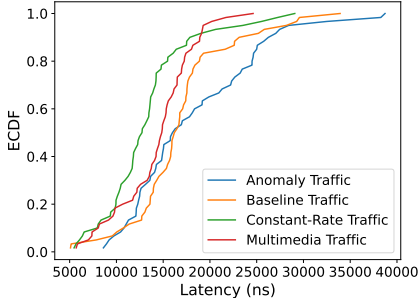
Resource allocation matters. The negative CPU coefficients in the quantile models highlight the importance of adequate CPU allocation for maintaining low-tail latencies. This relationship is visually reinforced in the CPU-latency scatter plot (Fig. 3c), where higher CPU availability is associated with consistently lower latencies, and low-CPU regions show both higher medians and markedly larger variances. The differences between the QFI values indicate that the QoS flows experience heterogeneous processing performance, which warrants further analysis of the interaction effects (CPU \times QFI, Packets \times QFI) in future studies.

Stable flows reduce latency. Relative to *Baseline* traffic, *Constant-Rate* lowers the median by -3.576ns (95% CI $[-4.950, -2.299]$ ns; $p_{\text{perm}} = 2 \times 10^{-4}$; Cliff's $\delta = -0.484$, large), while *Multimedia* reduces the median by -1.452ns (95% CI $[-2.772, -0.475]$ ns; $p_{\text{perm}} \approx 0.038$) and p95 by -8.907ns (95% CI $[-11.752, -1.519]$ ns; $p_{\text{perm}} \approx 0.014$); see Table V. These gains align with narrower IQRs for *Constant-Rate* and *Multimedia* (4.010ns and 4.736ns) versus *Anomaly* (10.684ns) in Table III, and with the steeper ECDF and slimmer violins in Figs. 3a–3b. Quantile regression (Table VI) shows negative CPU coefficients at p50 and p95 (e.g., p95: -4.10ns , $p \approx 0.038$), consistent with the downward trend and higher variance at low CPU values in Fig. 3c. Instability at p99 reflects rare but large outliers, rather than a systematic effect.

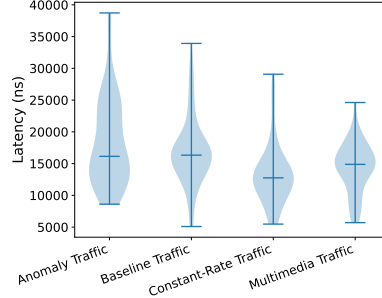
Consistency. Figs. 3a–3c confirm the statistics: the ECDF for *Constant-Rate* rises sharply (tight spread), while *Anomaly*'s heavier tail matches its larger IQR in Table III. Violin plots show a slim constant rate and a moderately wider multimedia, consistent with lower dispersion. The CPU-latency scatter concentrates the highest delays and variance at low CPU, aligning with the negative CPU coefficients and underscoring the need for resource headroom to control the tails.

VI. CONCLUDING REMARKS

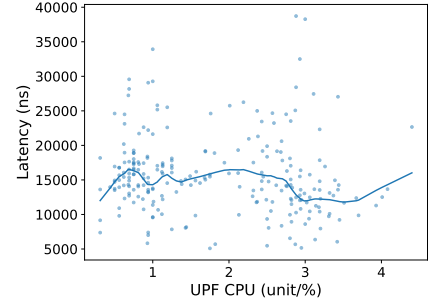
We presented a kernel level, per packet instrumentation for a container based UPF that attributes GTP-U decapsulation



(a) ECDF of UPF Processing Latency.



(b) Latency distribution (violin plots).



(c) Latency vs. CPU utilization.

Fig. 3: Latency characteristics across traffic classes and CPU load.

latency under NN conditions. Quantile regression shows that UPF CPU is the main lever for controlling latency tails, improving both typical and worst case delay. Heterogeneity across QFIs persists, and extreme tail inflation under contention reveals practical limits of slice isolation. Operators may keep CPU headroom at the UPF, favor rate stable shaping for latency sensitive flows, and monitor the UPF path with lightweight eBPF rather than only aggregate counters.

In future work, we will close the loop between per-packet telemetry and control for online NN mitigation, study interaction effects, extend the method to highly programmable dataplanes, and cover memory and network devices effects and eBPF overhead. Promising directions include telemetry-driven control that preserves the CPU headroom, priority-aware pacing, and earliest departure time scheduling to bound queuing for critical QFIs. Our findings pave the way for exploring high-fidelity isolation mechanisms for B5G networks.

ACKNOWLEDGMENT

The authors thank the FAPEMIG (Grant #APQ00923-24), FAPESP MCTIC/CGI Research project 2018/23097-3 - SFI2 - Slicing Future Internet Infrastructures. FCT has also supported this work – Fundação para a Ciência e Tecnologia within the R&D Unit Project Scope UID/00319/Centro ALGORITMI.

REFERENCES

- [1] Z. Zhong and R. Buyya, “A Cost-Efficient Container Orchestration Strategy in Kubernetes-Based Cloud Computing Infrastructures with Heterogeneous Resources,” *ACM Transactions on Internet Technology*, vol. 20, no. 2, pp. 1–24, Apr. 2020.
- [2] Z. Zhong, M. Xu, R. Buyya, C. Xu, and M. A. Rodriguez, “Machine Learning-based Orchestration of Containers: A Taxonomy and Future Directions,” *ACM Computing Surveys*, vol. 54, no. 10s, pp. 1–35, Jan. 2022.
- [3] M. Copik, M. Chrapek, L. Schmid, A. Calotoiu, and T. Hoefler, “Software resource disaggregation for hpc with serverless computing,” in *2024 IEEE International Parallel and Distributed Processing Symposium (IPDPS)*, 2024, pp. 139–156.
- [4] M. Golec, G. K. Walia, M. Kumar, F. Cuadrado, S. S. Gill, and S. Uhlig, “Cold start latency in serverless computing: A systematic review, taxonomy, and future directions,” *ACM Computing Surveys*, vol. 57, no. 3, Nov. 2024. [Online]. Available: <https://doi.org/10.1145/3700875>
- [5] R. Andreoli, R. Mini, P. Skarin, H. Gustafsson, J. Harmatos, L. Abeni, and T. Cucinotta, “A multi-domain survey on time-criticality in cloud computing,” *IEEE Transactions on Services Computing*, vol. 18, no. 2, pp. 1152–1170, 2025.
- [6] A. Donatti, S. L. Corrêa, J. S. B. Martins, A. J. G. Abelem, C. B. Both, F. de Oliveira Silva, J. A. Surugay, R. Pasquini, R. Moreira, K. V. Cardoso, and T. C. Carvalho, “Survey on machine learning-enabled network slicing: Covering the entire life cycle,” *IEEE Transactions on Network and Service Management*, vol. 21, no. 1, pp. 994–1011, 2024.
- [7] F. Muro, E. Baena, S. Fortes, L. Nielsen, and R. Barco, “Noisy neighbour impact assessment and prevention in virtualized mobile networks,” *IEEE Transactions on Network and Service Management*, vol. 20, no. 1, pp. 415–425, 2023.
- [8] J. X. S. Lozano, A. Garcia-Saavedra, X. Li, and X. C. Perez, “Airic: Orchestration of virtualized radio access networks with noisy neighbours,” *IEEE Journal on Selected Areas in Communications*, vol. 42, no. 2, pp. 432–445, 2024.
- [9] N. Yarkina, L. M. Correia, D. Moltchanov, Y. Gaidamaka, and K. Samouylov, “Multi-tenant resource sharing with equitable-priority-based performance isolation of slices for 5G cellular systems,” *Computer Communications*, vol. 188, pp. 39–51, Feb. 2022.
- [10] S. Luo, C. Lin, L. Zhang, K. Ye, G. Yang, H. Xu, C. Xu, and G. Xu, “Optimizing Resource Management for Shared Microservices: A Scalable System Design,” *ACM Transactions on Computer Systems*, vol. 42, no. 1-2, pp. 1–28, Feb. 2024.
- [11] S. Volpert, S. Winkelhofer, J. Domaschka, and S. Wesner, “Detecting noisy neighbors in cpu-isolated cgroups environments,” in *Proceedings of the 16th ACM/SPEC International Conference on Performance Engineering*, ser. ICPE ’25. New York, NY, USA: Association for Computing Machinery, 2025, p. 224–231. [Online]. Available: <https://doi.org/10.1145/3676151.3719376>
- [12] S. Hong, Y. Kim, J. Nam, and S. Kim, “On the analysis of inter-relationship between auto-scaling policy and qos of faas workloads,” *Sensors*, vol. 24, no. 12, 2024. [Online]. Available: <https://www.mdpi.com/1424-8220/24/12/3774>
- [13] T. Mukute, L. Mamushiane, A. A. Lysko, E.-R. Modroiu, T. Magedanz, and J. Mwangama, “Control Plane Performance Benchmarking and Feature Analysis of Popular Open-Source 5G Core Networks: OpenAir-Interface, Open5GS, and free5GC,” *IEEE Access*, vol. 12, pp. 113 336–113 360, 2024.
- [14] M. Andrade and J. Wickboldt, “A study on 5g network slice isolation based on native cloud and edge computing tools,” *Journal of Network and Systems Management*, vol. 33, no. 4, p. 90, Jul 2025. [Online]. Available: <https://doi.org/10.1007/s10922-025-09958-5>
- [15] M. Adeppady, P. Giaccone, H. Karl, and C. F. Chiasserini, “Reducing microservices interference and deployment time in resource-constrained cloud systems,” *IEEE Transactions on Network and Service Management*, vol. 20, no. 3, pp. 3135–3147, 2023.
- [16] B. M. da Silva, L. F. R. Moreira, R. Moreira, and F. de Oliveira Silva, “Leveraging infrastructure monitoring for user experience forecasting in container-based 5g core,” in *2025 Joint European Conference on Networks and Communications & 6G Summit (EuCNC/6G Summit)*, 2025, pp. 31–36.
- [17] I. Baldin, A. Nikolich, J. Griffioen, I. I. S. Monga, K.-C. Wang, T. Lehman, and P. Ruth, “FABRIC: A national-scale programmable experimental network infrastructure,” *IEEE Internet Computing*, vol. 23, no. 6, pp. 38–47, 2019.